Electron paramagnetic resonance study of paramagnetic defect centres Fe^{3+} and Cr^{3+} in $KTiOPO_4$

1991 J. Phys.: Condens. Matter 3 7877

(http://iopscience.iop.org/0953-8984/3/40/009)

J. Phys.: Condens. Matter 3 (1991) 7877–7886. Printed in the UK

Electron paramagnetic resonance study of paramagnetic defect centres Fe^{3+} and Cr^{3+} in $KTiOPO_4$

J M Gaite†, J F Stenger‡, Y Dusausoy‡, G Marnier‡ and H Rager§
† Laboratoire de Cristallographie, Unité associée au CNRS 810, Université d'Orléans, rue de Chartres, BP 6759, 45067 Orléans Cédex 2, France
‡ Laboratoire de Minéralogie et Cristallographie, Unité associée au CNRS 809, Université de Nancy I, BP 239, 54506 Vandoeuvre lès Nancy Cédex, France
§ Institute of Mineralogy, University of Marburg, Hans-Meerwein-Strasse, 3550 Marburg, Federal Republic of Germany

Received 8 February 1991, in final form 17 June 1991

Abstract. An EPR study of Fe^{3+} centres in single crystals of $KTiOPO_4$ (KTP) has been performed. Two crystals grown under identical conditions have been used in the experiment carried out at the Q-band frequency: the first was iron doped and the other was undoped. Four Fe^{3+} centres have been observed. All spin-Hamiltonian parameters were calculated for the four centres. Comparison of the pseudosymmetries obtained from fourth-order constants of the spin Hamiltonian and from a fourth-order crystal-field calculation for the two Ti octahedra allowed us to locate two Fe^{3+} centres at each Ti site in KTP. The absence of a strong axial deviation from cubic symmetry shows that the charge compensation mechanism is not at short distance for the four centres. All four cenres denoted as ST1, ST2, ST3 and ST4 are present in the iron-doped crystal but only one (ST4) is observable in the undoped crystal. In the undoped crystal, also Cr^{3+} was observed. Results for the Cr^{3+} centres are given and compared with those already reported by Hasanova and co-workers.

1. Introduction

The present focus of our research on $KTiOPO_4$ (KTP) is to study its defect chemistry. Knowledge of the individual defects and its properties may facilitate the understanding of physical properties of KTP. For example, the higher the defect concentration, the higher is the conductivity and the more susceptible KTP is to optical and electric field damage. This effect is explained on the basis of compensating mechanisms necessary to balance defects in the KTP lattice.

In a previous paper (Stenger *et al* 1989) we studied Fe^{3+} centres in KTP to find out which Ti site is substituted by Fe^{3+} and how the charge compensation occurs. In the investigated specimen, Fe^{3+} was located at the Ti(2) sites. According to the applied analysis of EPR and fourth-order crystal-field data the substitution of Ti^{4+} at Ti(2) by Fe^{3+} revealed nearly no lattice relaxation, indicating a long-range compensating mechanism.

0953-8984/91/407877 + 10 $03.50

In principle, the presence of impurities and defects in the KTP lattice gives rise to lattice relaxation which effects the efficiency of second-order processes, such as sum-and-difference frequency mixing and optical parametric oscillation. On the other hand, if defects and impurities are present only in a low concentration, they may not alter the physical properties very much but may be used as proper probes to test and to elucidate crystal growth processes. We, therefore, extended our research to the EPR study of two KTP single crystals one of which is nominally undoped (KTP1) and the other (KTP2) doped with iron in the parts-per-million region. The results are presented here.

2. Experimental procedure and analysis of data

The EPR measurements were performed at room temperature using a Varian Q-band spectrometer and 100 KHz modulation. The microwave frequency was calibrated using the resonance magnetic field of DPPH where the magnetic field scale (20 kG) was calibrated using a NMR gaussmeter. To study the accurate angular dependence of the EPR spectra, the crystal was oriented by the x-ray precession method and fixed inside the cavity in such a way that the investigated crystal plane was perpendicular to the rotation axis of the magnet. Small deviations of the crystal setting from the exact orientation could easily be identified by a splitting of the EPR signals. By adjustment of the crystal setting until the splitting vanished, a precise crystal orientation within $\pm 0.2°$ was established for all rotation measurements.

The EPR spectrum of Fe^{3+} is described by the general Hamiltonian (Abragam and Pryce 1951), for which no particular symmetry of the spin Hamiltonian is expected:

$$\mathcal{H} \sum_{ij} \beta B_i g_{ij} S_j + \sum_{m=-2}^{2} B_2^{\prime m} O_2^{\prime m} + \sum_{m=-4}^{4} B_4^{\prime m} O_4^{\prime m}. \tag{1}$$

g_{ij} $(i,j = X, Y, Z)$ are the components of the **g** tensor and $O_n^{\prime m}$ the normalized Stevens equivalent operators (Gaite 1987).

For all Fe^{3+} centres the 20 parameters of equation (1) are calculated using a computer program (Michoulier and Gaite 1972, Gaite and Michoulier 1973) which fits the solution of (1) to the experimental magnetic resonance fields.

To locate the Fe^{3+} ions in the KTP structure the method developed by Michoulier and Gaite (1972) and by Gaite and Michoulier (1973) is used. It is based on comparison of the pseudosymmetry axes of the fourth-order tensor $B_4^{\prime m}$ with the pseudosymmetry axes of the coordination polyhedron.

The fourth-order terms of the spin Hamiltonian are related to the fourth order of the crystal-field development (Hutchings 1964) because the nearest ligands contribute strongly to these terms. The pseudosymmetries are determined by the directions θ, ϕ of the n-fold pseudosymmetry axes and by the associated $\varepsilon_n(\theta, \phi)$ minimum values.

The fourth-order term

$$\mathcal{H}_4 = \sum_{-4}^{+4} B_m^{\prime 4} O_m^{\prime 4}$$

of the general spin Hamiltonian in equation (1) may be divided into a cubic and a

distorted part, i.e. $\mathcal{H}_4 = \mathcal{H}_{4,\,\mathrm{cubic}} + \mathcal{H}_{4,\,\mathrm{distorted}}$ (Gaite 1975). The cubic part is described by the parameter a' defined as

$$|a'| = 70\,|B_4'^0 + \sqrt{\tfrac{5}{7}}B_4'^4|_{\mathrm{Max}\,R(\alpha\beta\gamma)} = 70||B_4'^0| + \sqrt{\tfrac{5}{7}}\,[(B_4'^4)^2 + (B_4'^{-4})^2]^{1/2}|_{\mathrm{Max}\,R(0\beta\gamma)}$$

in which α, β and γ are the angles of the Euler rotation that brings the axes of the initial reference frame along the fourfold axes of the cubic part of $\mathcal{H}_4$. Thus, these angles describe fully the orientation of the 'cubic part' which is characteristic of the pseudocubic symmetry of $\mathcal{H}_4$. The deviation d of $\mathcal{H}_4$ from cubic symmetry is defined by

$$d = (a^{*2} - a'^2)/a^{*2}$$

with

$$a^* = 120\left(\tfrac{7}{12}\sum_{m=-4}^{4}(B_4'^m)^2\right)^{1/2}.$$

In the case of exact cubic symmetry, $a' = a^* = a$ where a is the usual cubic constant and d is zero.

The cubic part of $\mathcal{H}_4$ can be described in three-coordinate systems deduced from one another by circular permutation of the fourfold axes. In a plot of $B_4'^0$ versus $B_4'^4$, the description of $\mathcal{H}_4$ in these three reference systems will be represented by three points, having the following properties.

(i) The three points are on a straight line which is perpendicular to the 'cubic line' whose slope is $\sqrt{7/5}$.

(ii) The point representing the cubic part of $\mathcal{H}_4$ is at the intersection of the cubic line with the line joining the three plotted points.

(iii) The intersection of the two lines is the mass centre of the three plotted points.

The smaller the deviation from cubic symmetry, the closer the three points are to the 'cubic line'. It should be mentioned that, in this paper, fourfold symmetry was used for discussion but that the discussion is also possible on the basis of threefold symmetry.

3. Results and discussion

From the angular dependence of the EPR pattern measured in all three crystallographic planes of KTP2, four paramagnetic Fe^{3+} centres denoted as ST1, ST2, ST3 and ST4 could be distinguished. Centre ST2 corresponds to the centre described by Stenger *et al* (1989). The spectrum observed by Nizamutdinov *et al* (1987) has no correspondence with one of the four observed centres although it is very similar to the centres ST2 and ST4. For the centres ST1, ST2 and ST3 in KTP2, sufficient EPR transitions were observed to calculate the 20 parameters of the general spin Hamiltonian. For centre ST4 in KTP2 the intensity of the EPR transitions was so small that their angular dependence could not be followed up. Because in the specimen KTP1 centre ST4 occurs with sufficient intensity, the EPR angular dependence of ST4 was measured in the crystal KTP1. The standard deviations between the experimental and calculated magnetic transition fields are 14 G, 19 G, 11 G and 15 G for ST1, ST2, ST3 and ST4, respectively. This is inside the experimental accuracy because the angular dependence of the EPR transitions varies up to 300 G deg^{-1}.

Table 1. Fe^{3+} spin-Hamiltonian constants of the centres ST1, ST2, ST3 and ST4 in KTP. For comparison the data reported by Nizamutdinov *et al* are also included.

	ST1	ST3	ST2	ST4	Nizamutdinov *et al*
ij	Matrix components g_{ij}				
xx	1.9997	1.9995	2.0027	2.0027	
yy	2.0037	2.0055	2.0026	2.0045	
zz	2.0038	2.0045	2.0056	2.0048	
xy	−0.0015	0.0050	0.0009	0.0037	
xz	0.0003	−0.0019	−0.0011	0.0006	
yz	−0.0001	0.0000	−0.0008	0.0001	
m	Normalized second-order constants $B_2^{\prime m}$ (10^{-4} cm^{-1})				
0	261.5	278.6	167.5	200.3	147.2
1	314.1	117.0	−647.6	−621.0	177.8
−1	−334.5	−692.3	142.3	176.7	−642.6
2	264.0	411.7	−356.2	−338.4	343.3
−2	−126.6	−47.3	−139.3	−220.0	−135.0
m	Normalized fourth-order constants $60B_4^{\prime m}$ (10^{-4} cm^{-1})				
0	32.0	28.0	21.7	24.4	29.7
1	2.4	3.1	7.1	7.3	7.0
−1	10.0	9.8	3.2	3.8	10.2
2	−68.0	−50.2	47.1	56.9	−52.4
−2	−12.3	−4.9	17.2	18.7	17.0
3	2.2	−1.8	−18.5	−11.5	−4.9
−3	23.1	22.7	6.8	−2.9	14.8
4	−28.3	−19.2	−12.0	−18.0	−16.3
−4	−3.0	−2.9	−12.0	−16.3	12.6

For the centres ST1, ST2, ST3 and ST4 the values of g_{ij} and of the fine-structure constants $B_n^{\prime m}$ are given in table 1. The constants $B_n^{\prime m}$ are given in the crystallographic axes system which is defined as $X = a = 12.814$ Å, $Y = b = 6.404$ Å, $Z = c = 10.616$ in the $Pna2_1$ space group. The values of the second-order constants in their diagonal form and the orientation of the EPR axes in the crystal axes system are given in table 2. The stereographic projections of the EPR axes are shown in figure 1 from which two sets of centres each consisting of two components may be deduced.

The pseudosymmetry characteristics of all Fe^{3+} centres calculated as described above are presented in tables 3 and 4. In the same tables, we also give the pseudosymmetry characteristics of the fourth-order terms of the crystal field for the Ti(1) and Ti(2) octahedra, using the crystallographic data from Tordjman *et al* (1974). Of course this calculation reflects the pseudosymmetry characteristics of the undistorted polyhedra.

Figure 2 shows the stereographic projection of the fourfold pseudosymmetry axes of all ST centres. The data for the pseudosymmetries of ST2 and ST4 are so similar that they could not be drawn separately. Moreover, they agree well with the pseudosymmetry obtained from the crystal-field calculation for Ti(2). The pseudosymmetry data for ST1 and ST3 are also very similar and agree with the crystal field at Ti(1). Thus, the observed centres are supposed to be due to two centres at both Ti(1) and Ti(2) in agreement with

Table 2. Diagonal values of the second-order tensors and orientations of the eigenvectors in the crystal axes system. The data of Nizamutdinov *et al* are included for comparison.

	ST1		ST3		Nizamutdinov *et al*		ST2		ST4	
Stevens' constants B_2^0 (cm^{-1})	+0.055 98		−0.082 17		−0.072 59		−0.074 07		−0.071 92	
B_2^2 (cm^{-1})	+0.038 33		−0.044 37		−0.047 51		−0.044 29		−0.055 47	
$\lambda = B_2^2/B_0^2$	0.68		0.54		0.65		0.60		0.77	
	Orientation (deg) of EPR axes									
	θ	ϕ	θ	ϕ	θ	ϕ	θ	ϕ	θ	ϕ
Ox	120.1	12.6	102.5	7.7	113.14	14.15	110.3	78.4	116.6	80.2
Oy	68.8	89.6	148.3	118.7	138.5	133.0	40.1	139.1	41.6	135.9
Oz	141.8	150.0	61.4	90.8	57.6	88.8	58.6	2.7	60.6	6.5

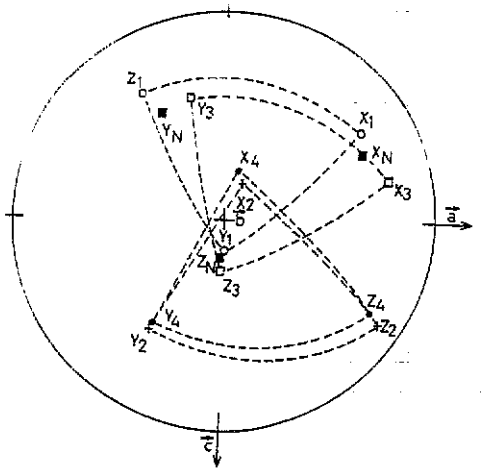

Figure 1. Stereographic projections of the EPR axes of the ST1, ST2, ST3 and ST4 centres and the data of Nizamutdinov *et al*.

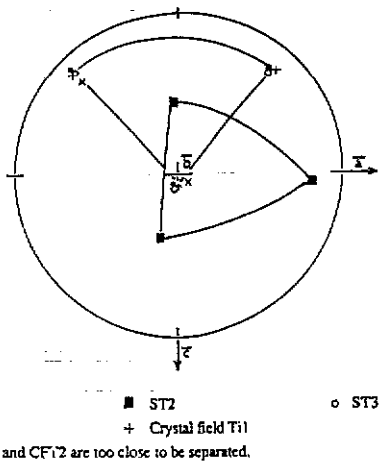

Figure 2. Stereographic projections of the pseudosymmetry axes of all ST centres.

the graph of the EPR axes in figure 1. The two EPR centres at Ti(1) as well as at Ti(2) differ in their EPR parameters (table 1); this is assumed to be due to differences in the charge compensation mechanisms at the particular Ti sites.

To illustrate the differences between the different EPR spectra in a clear way, the graphic representation of $B_4'^0$ versus $B_4'^4$ described above is used (figure 3). From this figure, it can be seen that the centres ST4 and ST3 are very similar and have a nearly axial distortion. This is also confirmed by their small ε-values for the third fourfold axis (tables 3 and 4). In contrast, the spectra for ST1 and ST2 differ significantly from those for ST3 and ST4 as well as from each other. Furthermore ST1 and ST2 deviate from cubic symmetry in the most general way.

From the pseudosymmetry data (figure 2) and the stereographic projection of the EPR axes (figure 1) it was concluded that the centres ST2 and ST4 are due to Fe^{3+} at Ti(2) whereas the centres ST1 and ST3 correspond to Fe^{3+} at Ti(1). This means that quite different Fe^{3+} centres occur at both Ti(1) and Ti(2) sites.

The results presented here are obtained from two different crystals KTP1 and KTP2 synthesized in the same way (Marnier 1986, 1988). The crystal KTP2, doped with 1000 ppm of Fe^{3+} in the growing bath was used for a preliminary study (Stenger *et al* 1989). In this sample, the most intensive spectrum was for ST2; the intensity of the ST4 spectrum was very low, and it was not possible to measure the angular dependences of its EPR transitions. The spectra for ST1 and ST3 were of about the same intensity. In the undoped crystal KTP1, only ST4 was observed; besides this centre, several other intensive EPR lines were also present. These lines could be identified as being due to two different Cr^{3+} centres. For these two spectra, in addition to the three allowed transitions which were always observed, $\Delta M = 2$ transitions were also present and were taken into account for the calculations. The spin-Hamiltonian constants of these two spectra centres (denoted as A and B in Table 5) were computed using the same method as for Fe^{3+}.

The characteristics of the spectra are given in table 5 together with those of the six spectra previously reported by Hasanova *et al* (1988). From this table, it is already evident that the spectrum for centre A corresponds to that for centre I. For centres II–

Table 3. Fe^{3+} at Ti(1).

	ST1		ST3		Nizamutdinov *et al*		Crystal field at Ti(1)	
	Orientations (deg) of the cubic part of the fourth-order tensors							
	θ	ϕ	θ	ϕ	θ	ϕ	θ	ϕ
	134.8	10.3	134.9	12.6	136.9	−1.2	135.8	9.6
	134.1	175.1	133.2	171.8	132.4	165.9	132.9	172.5
	82.3	92.5	79.3	91.9	83.5	81.9	81.3	90.7
	Characteristics of the cubic pseudosymmetry							
Norm (10^{-4} cm^{-1})	85.1		65.8		68.8			
$a^*/2$ (10^{-4} cm^{-1})	65.0		50.2		52.6			
$a'/2$ (10^{-4} cm^{-1})	63.3		48.8		49.9			
d (10^{-4} cm^{-1})	0.050		0.055		0.099		0.010	
	n-fold pseudosymmetry axes (θ and ϕ in degrees)							
n	1000ε	θ	ϕ	1000ε	θ	ϕ	1000ε	θ	ϕ	1000ε	θ	ϕ
4	21	134.9	10.6	21	134.9	12.7	98	136.9	−1.2	1.9	134.0	8.9
4	50	134.0	175.1	36	134.9	167.3	43	132.5	166.3	8.8	134.6	171.2
4	11	82.3	93.0	4	79.6	92.1	29	84.3	81.8	4.9	81.0	90.2
3	48	85.3	147.5	55	83.1	147.2	98	84.4	135.9	8.8	85.1	145.2
3	50	27.5	92.0	53	24.5	90.4	86	28.2	77.7	8.7	26.3	90.6
3	48	85.9	37.5	55	84.5	36.7	99	88.2	25.1	8.8	84.6	35.0
3	50	136.9	93.1	53	134.0	92.8	90	138.5	84.4	8.5	135.8	89.7

Table 4. Fe^{3+} at Ti(2).

	ST2		ST4		Crystal field at Ti(2)	
	Orientation (deg) of the cubic part of the fourth-order tensors					
	θ	ϕ	θ	ϕ	θ	ϕ
	136.6	91.2	135.7	94.6	137.2	92.5
	47.4	105.1	46.1	104.6	47.8	104.8
	82.9	8.7	85.0	9.8	83.9	9.2
	Characteristics of the pseudocubic symmetry					
Norm (10^{-4} cm^{-1})	61.0		70.6			
$a^+/2$ (10^{-4} cm^{-1})	46.6		53.9			
$a'/2$ (10^{-4} cm^{-1})	44.1		52.8			
d (10^{-4} cm^{-1})	0.103		0.039		0.009	
	n-fold pseudosymmetry axes (θ and ϕ in degrees)					
n	1000ε θ	ϕ	1000ε θ	ϕ	1000ε θ	ϕ
4	98 136.6	91.2	34 135.8	94.5	7.4 137.1	93.6
4	15 47.2	105.1	26 46.1	104.3	5.0 47.9	104.9
4	51 83.3	8.7	4 85.1	9.6	5.9 83.7	9.3
3	100 95.8	133.8	38 93.7	134.9	8.8 98.0	134.2
3	97 28.3	12.7	36 30.0	11.1	8.4 29.2	13.5
3	103 137.8	6.0	38 139.7	8.5	8.7 138.5	6.1
3	102 87.6	63.3	39 88.0	64.4	8.8 88.5	63.9

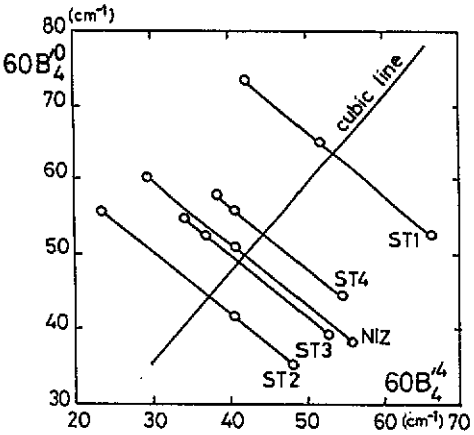

Figure 3. Distortion from cubic symmetry of all ST centres and the data of Nizamutdinov *et al* (NIZ).

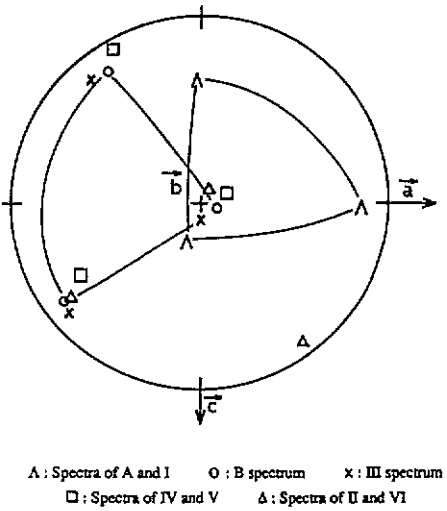

Figure 4. Cr^{3+} in KTP.

Table 5. Cr^{3+} in KTP. Diagonal values of the second-order tensors and orientations of the eigenvectors. Centres A and B are from the present work. Centres I–VI from Hasanova *et al* (1988) in our reference system.

	θ (deg)	ϕ (deg)	θ (deg)	ϕ (deg)		
	A		B			
Ox	67.5	98.4	126.1	−8.3		
Oy	157.4	94.9	36.3	−14.4		
Oz	88.8	7.9	87.1	79.5		
B_2^0 (cm^{-1})	0.1686		0.1373			
B_2^2 (cm^{-1})	0.0939		0.1197			
	I		II		VI	
Ox	68.2	98.1	126.0	−11.7	127.2	−11.1
Oy	158.1	92.7	37.0	5.8	38.6	6.7
Oz	88.2	7.4	98.0	84.7	98.7	85.6
B_2^0 (cm^{-1})	0.1681		0.1293		0.1218	
B_2^2 (cm^{-1})	0.0947		0.1227		0.120	
	III		IV		V	
Ox	130.3	−7.5	120.0	−19.6	117.9	−21.1
Oy	41.8	11.0	30.0	−5.9	28.6	−6.0
Oz	99.3	−89.5	95.8	73.6	96.3	72.3
B_2^0 (cm^{-1})	0.1139		0.1631		0.1629	
B_2^2 (cm^{-1})	0.124		0.1413		0.1327	

VI, we changed the labelling of axes in order to follow the general rule $|B_2^0| \geqslant |B_2^2|$, the two constants having the same sign. It must be remarked that, for centre B and centres II–VI, the ratio B_2^2/B_2^0 is nearly unity, which means that a small change in the crystal field may give an inversion of the Y and Z axes of the centre (centre III). Centre B is different from the others, but its characteristics are near the groups of centres II–VI. All these centres are surely Cr^{3+} at the same Ti position but with different charge compensation mechanisms. To illustrate this last point, the orientations of the EPR axes of the various centres are presented in figure 4 in the same reference frame as that used for Fe^{3+}. It must also be mentioned here that the spectrum for centre B may be one of the 11 spectra already observed by Hasanova *et al* (1990).

One interesting result of this study is that the distribution of Fe^{3+} centres in the doped and undoped crystals are very different. On the other hand, they are also different from that of the crystal studied by Nizamutdinov *et al* which was grown under other conditions. This is an indication that such studies may be helpful in the characterization of crystals.

References

Abragam A and Pryce H M L 1951 *Proc. R. Soc.* A **205** 135–52
Gaite J M 1975 *J. Phys. C: Solid State Phys.* **8** 3887–85
—— 1987 *Electron Magnetic Resonance of the Solid State* (Vancouver: Canadian Chemical Society) p 151
Gaite J M and Michoulier J 1973 *J. Chem. Phys.* **59** 488–92

Hasanova N M, Nizamutdinov N M, Izugzon A S, Bulka G R, Vinokurov V M, Pavlova N I and Rez I S 1988 *Physics of Minerals and Synthetic Crystals* p 87
—— 1990 Private communication
Hutchings M T 1964 *Solid State Physics* vol 16 (New York: Academic) pp 227–73
Marnier G 1986 *French Patent* CNRS 2609976 (29 July)
—— 1988 *US Patent* 4746396 (24 May)
Michoulier J and Gaite J M 1972 *J. Chem. Phys.* **56** 5205–13
Nizamutdinov N M, Hasanova N M, Bulka G R, Vinokurov V M, Rez I S, Garmash V M and Pavlova N I 1987 *Sov. Phys.–Crystallogr.* **32** 408–13
Stenger J F, Dusausoy Y, Marnier G, Rager H and Gaite J M 1989 *J. Phys.: Condens. Matter* **1** 4643–8
Tordjman I, Masse R and Guitel J C 1974 *Z. Kristallogr.* **139** 103–15